Molecular Bases of Cyclic and Specific Disulfide Interchange between Human ERO1α Protein and Protein-disulfide Isomerase

増井, 翔史

https://doi.org/10.15017/1441081

出版情報：九州大学, 2013, 博士（医学）, 課程博士
バージョン：
権利関係：やむを得ない事由により本文ファイル非公開（2）

Molecular bases of cyclic and specific disulfide interchange between human Ero1α and PDI

Shoji Masui[1], Stefano Vavassori[2], Claudio Fagioli[2], Roberto Sitia[2] and Kenji Inaba[1]

[1]Division of Protein Chemistry, Post-Genome Science Center, Medical Institute of Bioregulation, Kyushu University, 3-1-1 Maidashi, Higashi-ku, Fukuoka 812-8582, Japan

[2]Università Vita-Salute San Raffaele Scientific Institute, Division of Genetics and Cell Biology, Via Olgettina 58, I-20132 Milan, Italy

Running title: Specific Ero1α–PDI interplay

Address correspond to: Kenji Inaba; Division of Protein Chemistry, Post-Genome Science Center, Medical Institute of Bioregulation, Kyushu University, 3-1-1 Maidashi, Higashi-ku, Fukuoka 812-8582, Japan. Tel/Fax: +81-92-642-6433; e-mail: inaba-k@bioreg.kyushu-u.ac.jp

In the endoplasmic reticulum (ER) of human cells, Ero1α and protein disulfide isomerase (PDI) constitute one of the major electron-flow pathways that catalyze oxidative folding of secretory proteins. Specific and limited PDI oxidation by Ero1α is essential to avoid ER hyperoxidation. To investigate how Ero1α oxidizes PDI selectively among more than twenty ER-resident PDI-family member proteins, we performed docking simulations and systematic biochemical analyses. Our findings reveal that a protruding β-hairpin of Ero1α specifically interacts with the hydrophobic pocket present in the redox-inactive PDI b'-domain through the stacks between their aromatic residues, leading to preferred oxidation of the C-terminal PDI a'-domain. Ero1α associated preferentially with reduced PDI, explaining the stepwise disulfide shuttle mechanism, first from Ero1α to PDI and then from oxidized PDI to an unfolded polypeptide bound to its hydrophobic pocket. The interaction of Ero1α with ERp44, another PDI-family member protein, was also analyzed. Notably, Ero1α-dependent PDI oxidation was inhibited by a hyperactive ERp44 mutant that lacks the C-terminal tail concealing the substrate-binding hydrophobic regions. The potential ability of ERp44 to inhibit Ero1α activity may suggest its physiological role in ER redox and protein homeostasis.

Biological kingdoms have universally developed catalytic systems that generate disulfide bonds and introduce them into newly synthesized polypeptides to assist their productive folding (1,2). Almost all organisms, from bacteria to humans, are equipped with enzymes and redox compounds involved in these oxidative reactions. In the endoplasmic reticulum (ER) of eukaryotic cells, flavin adenine dinucleotide (FAD) plays a major role in supplying oxidative equivalents required for protein disulfide formation (3,4). Ero1 (ER oxidoreductin-1) is a highly conserved flavoenzyme that manufactures a disulfide bond in concert with FAD and transfers them

preferentially to protein disulfide isomerase (PDI) (5-8). PDI is an ER-resident member of the thioredoxin (Trx) superfamily containing two redox-active (a- and a'-domains) and two redox-inactive Trx-like domains (b- and b'-domains). According to the crystal structures of yeast PDI (Pdi1p), these four Trx-like domains are lined up in the order a-b-b'-a', assuming different spatial arrangements, 'twisted U-shape' or 'boat' (9,10). Additionally, PDI conserves an α-helical domain (c-domain) and a linker loop (x-linker) at the C-terminus and between the b'- and a'-domains, respectively.

Recent studies on yeast and human Ero1s revealed not only their atomic resolution structures but also their regulation mechanisms (11-14). Since the generation of each disulfide bond by Ero1 is accompanied by the production of one molecule of hydrogen peroxide, a potential source of reactive oxygen species (ROS) (15), its enzymatic activity is tightly regulated in living cells. Indeed, yeast Ero1p exerts a feedback regulation mechanism, in which oxidation or reduction of two non-catalytic cysteine pairs (Cys90-Cys349 and Cys150-Cys295) presumably restricts the motion of the loop containing the electron shuttle disulfide (Cys100-Cys105), thereby modulating PDI oxidation activity (16). A similar mechanism is likely to operate in human Ero1α (17,18) and another Ero1 isoform, Ero1β (19). Human Ero1α has four regulatory cysteines (Cys94, Cys99, Cys104, and Cys131) whose rearrangements regulate oxidative activity: active Ero1α (Ox1) contains the Cys94-Cys99 disulfide while an inactive isoform (Ox2) possesses the Cys94-Cys131 and possibly Cys99-Cys104 disulfides. Accordingly, constitutively active (referred to as "hyperactive" in this paper) and inactive forms of Ero1α were prepared by introducing the mutation of Cys104&131Ala and that of Cys99&104Ala into this enzyme, respectively (12,18). Crystal structures of hyperactive and inactive forms of human Ero1α suggested that while their overall structures are almost the same, the different combination pattern between the regulatory cysteines positioned in an intrinsically flexible loop enables the fine-tuning of the electron shuttle ability of the loop (12). In hyperactive Ero1α, the Cys94-Cys99 pair could readily transfer electrons from PDI to the FAD-proximal active-site disulfide (Cys394-Cys397), leading to its high oxidative activity.

More recently, it was found that hydrogen peroxide can be utilized for protein disulfide bond formation in mammalian cells. An ER-localized peroxiredoxin (Prx) isoform, Prx4, metabolizes hydrogen peroxide by reducing it to a water molecule through the oxidation of the active-site free thiols (20). Oxidized Prx4, in turn, engages in oxidation of PDI, leading to the recycling of this enzyme and hence the establishment of a novel catalytic pathway for disulfide formation in the ER (21,22). In addition to this, catalytic oxidation by the quiescin sulphydryl oxidases (23), vitamine K epoxide oxidoreductase (24), GPx7 and 8 (25), and even direct oxidation by low-molecular weight compounds such as hydrogen peroxide (26) and dehydroascorbate (27) may also function as alternative catalysts to sustain disulfide bond formation in mammalian cells. These findings can explain how disruption of both Ero1α and Ero1β only modestly delays oxidative folding in mammalian cells (28).

Despite the plausible existence of the multiple oxidative pathways, it remains an essential issue how Ero1 can oxidize PDI specifically. To date, more than twenty oxidoreductases of the PDI family have been identified in the ER of mammalian cells (29,30). If Ero1 could oxidize PDI family member proteins in a non-specific and unregulated manner, the resulting hyperoxidizing ER environment would disallow isomerization or reduction of incorrectly formed disulfide bonds. Eventually, misfolded proteins would accumulate excessively. As another harmful effect of unregulated Ero1 catalysis, hydrogen peroxide could be generated over the capacity of the cellular antioxidant defense system, resulting in oxidative stress and ultimately apoptosis (31-33). To avoid futile oxidation cycles in the ER, therefore, Ero1 acquired the ability to recognize PDI preferentially.

Human Ero1α preferentially oxidizes the C-terminal Trx-domain (a'-domain) of human PDI (18,34). Recent biochemical works by others and us clarified that the PDI b'-domain contains the elements essential for the effective and specific oxidation by Ero1α (12,35). Indeed, mutual swapping of the b'-domain between PDI and ERp57, an oxidoreductase with a similar a-b-b'-a' domain arrangement (36), strikingly converted their reactivity and affinity for Ero1α (12). However, little is known about the molecular basis of Ero1α-PDI b'-domain recognition and how this interaction is regulated during the Ero1α catalysis of PDI oxidation. To address these issues, we initially modeled the Ero1α-PDI complex *in silico* and then, confirmed it by means of systematic biochemical analyses in accordance with the predicted complex structure model. Our data revealed that the protruding β-hairpin in Ero1α specifically binds the hydrophobic pocket in the b'-domain in a manner dependent on the PDI redox state, ensuring a specific and effective oxidative pathway.

Ero1α also binds ERp44, a PDI family protein that retains intracellularly Ero1α and other client proteins (37-39). We show here that ERp44 binds Ero1α even in the absence of the protruding β-hairpin interacting with PDI. By contrast, an ERp44 variant with increased substrate-binding capacity inhibited the Ero1α catalysis of PDI oxidation. These findings may highlight a novel regulatory role of ERp44 in ER redox and protein homeostasis.

EXPERIMENTAL PROCEDURES

Preparation of human Ero1α, PDI and ERp44- Ero1α and PDI mutants used in this work were constructed using a Quik Mutagenesis Kit (Stratagene) with appropriate primer sets. The overexpression and purification of hyperactive (with the mutations of Cys104 & 131 Ala) or Δ272-274 (with the deletion of the 272-274 segment) Ero1α lacking the non-functional cysteine Cys166 and PDI were performed essentially as described in (12). For preparation of recombinant human ERp44, a cDNA lacking the signal sequence was subcloned into the *NheI-Xho*I site of the pET28b vector (Novagen). An ERp44 mutant that lacks the C-terminal tail (ΔTail ERp44) was constructed by inserting a stop codon after Glu330. WT and ΔTail ERp44 were overexpressed in *E. coli* strain BL21(DE3). Cells were grown at 20°C in Luria-Bertani (LB) medium containing 50 μg/ml ampicillin, and

isopropyl-β-D-thiogalactoside (IPTG) was added at a final concentration of 0.5 mM at A_{600} = ~ 0.5. After continuous shaking at 20°C overnight, cells were harvested. The cell lysate supernatant was applied to the Ni-NTA Sepharose open column. Fractions eluted with 200 mM imidazole were further purified by anion exchange chromatography with a MonoQ column. ERp44 thus purified was quantified using the BCA method.

Surface plasmon resonance (SPR) measurement- The association and dissociation rate constants (k_{on} or k_{off}) for the direct binding of PDI or ERp44 to immobilized Ero1α were determined by SPR measurements on a BIACORE2000 system (GE Healthcare), as described in (12). The hyperactive or Δ272-274 Ero1α variants were coupled to the CM5 sensor chip (GE Healthcare) using amine-coupling chemistry. As a control, one channel was coupled with bovine serum albumin (BSA) to exclude background binding. The running buffer was 20 mM HEPES-NaOH (pH 7.4), 150 mM NaCl, 0.001% Tween-20, 2 mM EDTA, 1 mM GSH, and 0.25 mM GSSG (reducing condition) or 2 mM GSSG (oxidizing condition). All analyte samples were exchanged and diluted into each running buffer beforehand. Sensorgrams were analyzed by nonlinear regression analysis according to a two-state model using the BIAevaluation 4.1 software. Experiments were replicated at least three times.

Oxygen consumption assay- Oxygen consumption was measured using a Clark-type oxygen electrode (YSI 5331) as described in (12). All experiments were performed at 30°C in air-saturated buffer (~235 μM O_2) in 50 mM Tris-HCl (pH 8.1), 150 mM NaCl. Catalytic oxygen consumption was initiated by adding each Ero1α construct to a final concentration of 2 μM in a reaction mixture containing 10 μM PDI or its derivatives and 10 mM GSH.

Circular dichroism (CD) measurements- CD spectra in the far UV region of Ero1α and its mutants were recorded using JASCO J-720. The buffer used was 20 mM sodium phosphate (pH8.0), 100 mM NaCl. Sample concentration was 2 μM, and the light path of the cuvette was 1 mm.

J chain (JcM) refolding assays and immunoprecipitation- The *in vivo* JcM refolding assay was performed essentially as described in (40). Briefly, HeLa cells transfected with Myc-tagged J chain (JcM) in combination with Ero1α (hyperactive or Δ272-274) or ERp44 (WT or ΔTail) using Lipofectin (Invitrogen) were incubated for 5 min at 37 °C with 5 mM DTT in Optimem, to reduce intracellular disulfide bonds. After quick wash with PBS at 4 °C, cells were cultured in D-MEM (5% FCS) at 20 °C without DTT and quenched with 10 mM N-ethylmaleimide (NEM) at different time points to block disulfide interchange reactions. Cells were lysed in RIPA buffer with 10 mM NEM and protease inhibitors, and post nuclear supernatants harvested by centrifugation at 4 °C. Western blots were decorated with 9E10 anti-Myc, anti-J chain or anti-HA antibodies followed by a HRP-conjugated secondary antibody.

For isolation of Ero1α-ERp44 complexes and ERp44-PDI, aliquots of the cell lysates

(corresponding to $2x10^6$ cells) were IPed with anti-Myc (9E10), immobilized on Protein A beads and washed three times with STN buffer (20 mM Tris-Cl pH 7.7, 150 mM NaCl , 0.25% NP-40).

Results

Docking modeling of Ero1α-PDI non-covalent complexes- We previously observed that a PDI mutant in which all four redox-active cysteines in the a- and a'-domains were mutated to alanine bound Ero1α with almost the same association and dissociation kinetics as wild-type PDI, suggesting that Ero1α and PDI form a binary complex mainly through non-covalent interactions (12). We sought to model the Ero1α-PDI interaction *in silico* employing the currently available crystal structure of full-length Ero1α (PDB ID: 3AHQ) and the solution structure of the b-b' domain fragment of human PDI (PDB ID: 2K18). Our docking simulation was carried out on the website (http://sysimm.ifrec.osaka-u.ac.jp/surFit/), analyzing the molecular surface, electrostatic potential and hydrophobicity complementarity, weighted by the conservation of interacting residues (41,42). Numerous complex models were predicted and ranked: among these, a model with the second highest score was consistent with our previous findings suggesting that the hydrophobic pocket in the b'-domain is involved in Ero1α binding. As illustrated in Fig. 1A & 1B, this model suggested that the hydrophobic pocket including Phe240, Phe249 and Phe304 accommodates a protruding β-hairpin region of Ero1α, ensuring the non-covalent interaction between these two enzymes. In particular, Ero1α Trp272 seems to play the most critical role in this molecular recognition, with its indole ring closely contacting aromatic or hydrophobic residues in PDI (see also the next section).

Importantly, when the PDI a'-domain is extensionally placed next to the b'-domain based on the crystal structure of full-length yeast PDI (9), its redox-active site is predicted to reside in close proximity to the electron-shuttle loop of Ero1α (Fig. 1A), consistent with previous observations that human Ero1α preferentially and effectively oxidizes the PDI a'-domain (18,34,35). While the overall structures of yeast Ero1p and human Ero1α are similar except for the regions regulating PDI oxidation activity (see Ref. 12 for more details), the protruding β-hairpin region is shorter in yeast Ero1p (Fig. 1C & Supplemental Fig. S1). This structural difference suggests different interaction modes between the yeast and human Ero1-PDI systems (see also Discussion).

Critical residues in the functional Ero1α-PDI interplay- To confirm and provide physiological significance of the predicted complex, we performed extensive biochemical and biophysical analyses. First, we constructed an Ero1α mutant lacking the protruding β-hairpin (Δ272-274) and analyzed its affinity for PDI by SPR under a redox condition mimicking that found in the ER (GSH:GSSG ratio of 4:1). PDI exhibited prominent binding to immobilized hyperactive Ero1α, with association and dissociation rates of 2.0 x 10^3 $M^{-1}s^{-1}$ and 4.1 x 10^{-3} s^{-1}, respectively (Fig. 2A, left). The 'dissociation constant (K_D) for hyperactive Ero1α' of PDI was approximately 2.1 μM. Conversely,

Δ272-274 Ero1α showed much smaller increases of the response signal, even when high PDI concentrations (8, 16 and 32 μM) were injected (Fig. 2A, right). The CD spectrum in far UV region excluded gross folding defects for Δ272-274 Ero1α (Fig. 2E). Altogether, these results indicated that the interaction between Ero1α and PDI was substantially impaired by the deletion of the protruding β-hairpin loop *in vitro*.

Next, to examine the role of the identified complex formation in Ero1α catalysis of PDI oxidation, we replaced Phe240, Phe249 or Phe304, a residue constituting the hydrophobic pocket, with a negatively charged glutamate, and measured oxygen consumption during oxidation of the PDI mutants by hyperactive Ero1α. As shown in Fig. 2B, whereas F249E PDI was oxidized by Ero1α at almost the same rate as WT PDI, oxidation of F240E PDI was slowed down to a large extent. The F304E mutation also negatively affected the reactivity of PDI against Ero1α albeit to a lesser extent than F240E. The results strongly suggest that Phe240 and possibly Phe304 in the PDI b'-domain are responsible for the functional interaction with Ero1α.

Similarly, we confirmed the role of the protruding β-hairpin of Ero1α in PDI oxidation. The Δ272-274 Ero1α consumed oxygen much more slowly than hyperactive Ero1α (Fig. 2C), indicating the necessity of the protruding β-hairpin in effective PDI oxidation.

As addressed in the previous section, the complex model suggested that the indole ring of Trp272 closely contacts phenylalanines located in the PDI-b' hydrophobic pocket. To investigate its role in PDI oxidation, we mutated Trp272 to residues with different volume and/or polarity. While replacement with an aromatic phenylalanine compromised Ero1α activity only slightly, more severe inactivation was observed upon substitution to Glu, Gly or Leu (Fig. 2D). The mutations at Trp272 did not affect the overall structure of Ero1α (Fig. 2E). Taken together, the results suggest that Trp272 of Ero1α interacts with Phe240 and to a lesser extent Phe304 of PDI through the stacks between their aromatic side chains, leading to effective catalysis of PDI oxidation, as predicted by our molecular docking.

Ero1α-PDI interaction in living cells- To further explore the physiological significance of the Ero1α-PDI interaction, we monitored oxidative folding of J chain (JcM) in living cells expressing WT or Δ272-274 Ero1α (40). In this assay (Fig. 3A), the *in vivo* activity of Ero1α can be assessed by the appearance of high molecular weight covalent complexes (HMWC), the compaction of JcM homodimers (Dim.) and the kinetics of disappearance of reduced JcM (Red., see Fig. 3B for a densitometric quantification). Reduced JcM disappeared more rapidly in WT Ero1α than in Δ272-274 transfected cells, despite the two transgenes were similarly expressed (Fig. 3C). These results strongly suggest that the protruding β-hairpin of Ero1α plays an important role in catalyzing JcM oxidation in living cells. Consistently, the deletion of this region substantially, but not completely, abolished the Ero1α activity *in vitro* (Fig. 2C), implying the existence of other minor molecular determinants ensuring the interaction between Ero1α and PDI. In agreement with this notion, covalent Δ272-274 Ero1α-PDI complexes were detected, albeit in

smaller amounts than with WT Ero1α (Fig. 3D). Notably, the Ero1α Ox1/Ox2 ratio in cells coexpressing PDI was slightly but significantly lower in Δ272-274 than in WT transfectants (Fig. 3D & 3E). These results suggest that interactions with PDI could contribute to the Ox1-Ox2 interconversion of Ero1α. While multiple interaction modes may occur between Ero1α and PDI (see also Discussion), our extensive *in vivo* studies confirmed the key role of the protruding β-hairpin in the functional Ero1α-PDI interplay.

Redox dependency of the Ero1α-PDI interaction- To ensure efficient recycling, PDI needs to dissociate from Ero1α after it is oxidized. This implies that the 'affinity for Ero1α' of PDI be dependent on its redox state. We investigated this possibility by measuring the association and dissociation kinetics of PDI against Ero1α under reducing and non-reducing conditions. As shown in Fig. 4A, a large fraction of WT PDI was reduced in a buffer containing 1mM GSH/0.25 mM GSSG, while it was fully oxidized in 2mM GSSG as was in 10mM potassium ferricyanide. On the other hand, hyperactive Ero1α remained mostly oxidized also in the presence of 1 mM GSH/0.25 mM GSSG.

Notably, while the association phase was not significantly affected, the dissociation of WT PDI from Ero1α was much faster at 2mM GSSG than at 1mM GSH/0.25 mM GSSG (Fig. 4B). As a result, oxidized PDI had a >10-fold lower affinity for Ero1α than reduced PDI. This was further confirmed by SPR measurements employing Cys-less PDI with both the CXXC motifs in the a- and a'-domains replaced by AXXA, as a mimic of constitutively reduced PDI. Differently from WT PDI, the association and dissociation kinetics of Cys-less PDI were essentially insensitive to the redox condition (Fig. 4B). These results suggest that formation and cleavage of the redox-active disulfides induce conformational changes in PDI, thereby modulating its affinity for Ero1α (see also Discussion).

Different binding modes of Ero1α toward ERp44 and PDI- ERp44 is a multifunctional chaperone of the early secretory pathway that interacts with Ero1α, Ero1β and other substrate proteins (39,43), favoring their intracellular retention (38). While ERp44 associates with Ero1α at almost the same rate as PDI, its dissociation was much faster (Fig. 5A and 2A). As a result, the 'K_D for Ero1α' of ERp44 was approximately 20-fold higher than that of PDI. Since ERp44 exhibited similar binding toward Ero1α even upon the mutation of its redox-active cysteine (Cys29) to alanine (Vavassori et al., manuscript submitted for publication)(37,44), the binding curve observed herein is primarily ascribed to non-covalent interactions.

In sharp contrast to PDI, however, ERp44 bound Δ272-274 Ero1α as tightly as hyperactive Ero1α (Fig. 5A), its association and dissociation kinetics being unaffected by the presence or absence of the protruding β-hairpin. Accordingly, co-immunoprecipitation experiments revealed that Δ272-274 and WT Ero1α similarly interacted with ERp44 (Fig. 5B, lanes 1 and 2), whilst the former mutant precipitated less PDI than the latter (Fig. 5B, lanes 3 and 4). These results strongly suggest that the protruding β-hairpin of Ero1α is not important for

interaction with ERp44. The different modes in the PDI-Ero1α and ERp44-Ero1α interactions were further supported by oxygen consumption assays. An excess of ERp44 (50 μM ERp44 vs 10 μM PDI) only slightly inhibited the Ero1α catalysis of PDI oxidation (Fig. 5C). However, a hyperactive ERp44 mutant lacking the auto-inhibitory C-tail (ΔTail) and hence possessing increased substrate-binding capacity (45), markedly inhibited PDI oxidation (Fig. 6A). Overexpression of ΔTail ERp44 significantly delayed JcM refolding, WT ERp44 having instead only marginal effects (Fig. 6B). SPR analyses confirmed that ΔTail ERp44 showed ~20-fold higher association rates and hence affinity for Ero1α (Fig. 6C left). The interaction between ΔTail ERp44 and Ero1α was not significantly affected by deleting the protruding β-hairpin region in Ero1α (Fig. 6C right), consistent with the notion that PDI and ERp44 interact with Ero1α with different modes. It is conceivable that without its C-terminal tail, ERp44 constitutively expose the redox-active Cys29 and surrounding hydrophobic patches. Its enhanced binding to Ero1α would restrain the PDI oxidation activity. We thus propose that ERp44 has the potential to regulate the Ero1α-PDI interplay in the cell (see also Discussion).

Discussion

Our work identifies the primary binding site between Ero1α and PDI: the protruding β-hairpin of Ero1α and the hydrophobic pocket in the PDI b'-domain non-covalently interact with each other through the stack between several aromatic residues. Modeling of the complex between the two proteins predicts that the PDI a'-domain will be suitably located for disulfide exchange with the Cys94-Cys99 disulfide present in the Ero1α shuttle loop (Fig. 1A), accounting for its preferential oxidation. These findings are consistent with our previous observations that not only small peptides (somatostatin and mastoparan) that bind the PDI hydrophobic pocket but also a detergent (Triton X-100) that decreases interactions of the peptides with PDI (46) significantly inhibited the Ero1α-catalyzed PDI oxidation (12). Since reduced PDI can exert chaperone activity (47), the extended conformation of the protruding β-hairpin in Ero1α could mimic a part of a misfolded or unfolded protein. Interestingly, Δ272-274 Ero1α accumulated less Ox1 in the presence of overexpressed PDI than WT Ero1α. Thus, the complex formation characterized in this study is presumably advantageous for the selective oxidation of PDI a'-domain by Ero1α, the chaperone activity of reduced PDI facilitating Ero1α Ox1-Ox2 interconversion.

Noticeably, Trp272 located at the edge of the protruding β-hairpin plays a pivotal role in the functional Ero1α-PDI interplay. Accordingly, previous NMR analyses revealed closed contacts of aromatic residues in somatostatin (AGSKNFFWKTFTSS) or a shorter peptide (KFWWFS) with the hydrophobic pocket in the PDI b'-domain (48,49). Moreover, the crystal structure of a PDI b'-x fragment demonstrated that Trp364 contained in the x-linker segment can bend and accommodate into the b' hydrophobic pocket surrounded by Phe240, Phe249 and Phe304 (supplemental Fig. S2), as does Ero1α Trp272 in the modeled complex (Fig. 1B).

Multiple Ero1 sequence alignments reveal

highly conserved aromatic residues (tryptophane or phenylalanine) at this position (Supplemental Fig. S1), suggesting that the Ero1-PDI interplay proposed in this work may be a common feature in high eukaryotes. However, the Ero1-PDI systems in *Arabidopsis thaliana* and fungi likely adopt a different interaction mode for the following reasons. First, Ero1 proteins from these species are predicted to lack the protruding β-hairpin and an aromatic residue corresponding to Trp272 of human Ero1α (Supplemental Fig. S1). Second, the rate of Pdi1p oxidation by yeast Ero1p was not affected by addition of somatostatin or mastoparan (50). Third, unlike human Ero1α, yeast Ero1p oxidizes the N-terminal Trx domain (a-domain) of yeast Pdi1p more effectively than its C-terminal a'-domain (50). Nonetheless, human Ero1α rescued the *ero1-1* yeast temperature sensitive mutant (40): the cross oxidation of yeast Pdi1p by human Ero1α might reflect the existence of a hydrophobic pocket in the b'-domain of yeast Pdi1p as well (9). Ero1 and PDI may have acquired higher reciprocal specificity, presumably as the number of oxidoreductases increased. Yet, this oxidative system seems to retain some plasticity as a trace of its evolution.

It remains to be seen whether the interaction mode identified herein is the sole that drives the electron flow from PDI to Ero1α in cells. Deletion of the protruding β-hairpin compromised, but did not completely abolish, the ability of Ero1α to oxidize PDI *in vitro* and to promote *in vivo* JcM folding. Additionally, some disulfide-linked Ero1α-PDI complex accumulated in cells expressing Δ272-274 Ero1α. CD analyses argue against this being due to misfolding of the mutant. Thus, additional interactions can mediate PDI recognition and oxidation.

Having elucidated the primary interaction mode between monomeric Ero1α and PDI at the amino acid level, a key open question remained as to how the 'affinity for Ero1α' of PDI is regulated to allow rapid and efficient cycles of electron transfer to cargo proteins. Our SPR analyses demonstrated that human PDI tends to dissociate from Ero1α upon oxidation of its redox active sites. As a consequence, the 'affinity for Ero1α' is more than 10-fold lower for oxidized than for reduced PDI. Recent analyses revealed that oxidation of the active site of the PDI a'-domain induced the spatial rearrangement of the b'- and a'-domains through the conformational change of the x-linker region, leading to enhanced exposure of the substrate-binding hydrophobic surface and significant changes in the solvation pattern (51,52). Consistently, the mobile x-linker region (53,54) could regulate substrate binding. These structural features suggest that the different 'affinity for Ero1α' of oxidized and reduced PDI might reflect redox-dependent changes in shape, space and solvation of the hydrophobic surface of PDI. In other words, the spatial position of the a'-domain relative to the b'-domain could be a crucial factor that determines whether PDI preferably binds Ero1α or unfolded/misfolded polypeptides; the more exposed hydrophobic pocket in oxidized PDI could accommodate unfolded substrates of overall extended configurations more preferentially than Ero1α of a globular fold. On the basis of these findings, we propose a comprehensive model of the

Ero1α-PDI catalytic pathway that drives oxidative protein folding in human cells (Fig. 7).

Additional ER-resident proteins and compounds could regulate the Ero1α-PDI pathway. Indeed, we found that ERp44 binds Ero1α differently from PDI, the Ero1α β-hairpin being disposable for the interaction. Unlike wild type ERp44, the hyperactive ΔTail mutant partially inhibited Ero1α-dependent PDI oxidation. Deletion of the auto-inhibitory C-terminal tail, and thus an unregulated exposure C29 and surrounding of hydrophobic patches, made ERp44 a stronger binder for Ero1α than PDI (Fig. 6C). The regulated activity of ERp44 *in vitro* and *in vivo* (45; Vavassori et al., submitted) could thus be an additional factor for controlling oxidative folding in the early secretory compartment.

In conclusion, the molecular basis underlying the specific and regulated Ero1α-PDI oxidative pathway has now been understood in greater details. The accumulating knowledge of the mechanisms of operation and regulation in protein disulfide bond formation systems will provide further important insights into the protein and redox homeostasis in the cell.

Acknowledgements

We thank Kengo Kinoshita for help in the docking simulation, Kazutaka Araki and Kazuhiro Nagata for helpful advice on the oxygen consumption and SPR measurements, and Gloria Bertoli and Margherita Cortini for helpful suggestions. We are also grateful to Hiroka Iida and Akiko Sato for technical support. This work was supported by a Grant-in-Aid for Young Scientists (A) from MEXT and the Yamada Science Foundation (to K. Inaba) and Regione Lombardia (ASTIL) and Associazione Italiana Ricerca Cancro (AIRC) (to R.Sitia).

References

1. Inaba, K. (2010) *Genes Cells* **15**, 935-943
2. Depuydt, M., Messens, J., and Collet, J. F. *Antioxid. Redox Signal.* **in press**
3. Tu, B. P., and Weissman, J. S. (2004) *J. Cell Biol.* **164**, 341-346
4. Thorpe, C., and Coppock, D. L. (2007) *J. Biol. Chem.* **282**, 13929-13933
5. Frand, A. R., and Kaiser, C. A. (1998) *Mol. Cell* **1**, 161-170
6. Pollard, M. G., Travers, K. J., and Weissman, J. S. (1998) *Mol. Cell* **1**, 171-182
7. Cabibbo, A., Pagani, M., Fabbri, M., Rocchi, M., Farmery, M. R., Bulleid, N. J., and Sitia, R. (2000) *J. Biol. Chem.* **275**, 4827-4833
8. Mezghrani, A., Fassio, A., Benham, A., Simmen, T., Braakman, I., and Sitia, R. (2001) *EMBO J.* **20**, 6288-6296
9. Tian, G., Xiang, S., Noiva, R., Lennarz, W. J., and Schindelin, H. (2006) *Cell* **124**, 61-73
10. Tian, G., Kober, F. X., Lewandrowski, U., Sickmann, A., Lennarz, W. J., and Schindelin, H. (2008) *J. Biol. Chem.* **283**, 33630-33640
11. Gross, E., Kastner, D. B., Kaiser, C. A., and Fass, D. (2004) *Cell* **117**, 601-610
12. Inaba, K., Masui, S., Iida, H., Vavassori, S., Sitia, R., and Suzuki, M. (2010) *EMBO J.* **29**, 3330-3343
13. Sevier, C. S., and Kaiser, C. A. (2008) *Biochim. Biophys. Acta* **1783**, 549-556
14. Tavender, T. J., and Bulleid, N. J. (2010) *Antioxid. Redox Signal.* **13**, 1177-1188
15. Gross, E., Sevier, C. S., Heldman, N., Vitu, E., Bentzur, M., Kaiser, C. A., Thorpe, C., and Fass, D. (2006) *Proc. Natl. Acad. Sci. U.S.A.* **103**, 299-304
16. Sevier, C. S., Qu, H., Heldman, N., Gross, E., Fass, D., and Kaiser, C. A. (2007) *Cell* **129**, 333 - 344
17. Appenzeller-Herzog, C., Riemer, J., Christensen, B., Sorensen, E. S., and Ellgaard, L. (2008) *EMBO J.* **27**, 2977-2987
18. Baker, K. M., Chakravarthi, S., Langton, K. P., Sheppard, A. M., Lu, H., and Bulleid, N. J. (2008) *EMBO J.* **27**, 2988-2997
19. Wang, L., Zhu, L., and Wang, C. C. (2011) *Biochem. J.* **434**, 113-121
20. Tavender, T. J., Sheppard, A. M., and Bulleid, N. J. (2008) *Biochem. J.* **411**, 191-199
21. Zito, E., Melo, E. P., Yang, Y., Wahlander, A., Neubert, T. A., and Ron, D. (2010) *Mol. Cell* **40**, 787-797
22. Tavender, T. J., Springate, J. J., and Bulleid, N. J. (2010) *EMBO J.* **29**, 4185-4197
23. Kodali, V., and Thorpe, C. (2010) *Antioxid. Redox Signal.* **13**, 1217-1230
24. Li, W., Schulman, S., Dutton, R. J., Boyd, D., Beckwith, J., and Rapoport, T. A. (2010) *Nature* **463**, 507-512
25. Nguyen, V. D., Saaranen, M. J., Karala, A. R., Lappi, A. K., Wang, L., Raykhel, I. B., Alanen, H. I., Salo, K. E., Wang, C. C., and Ruddock, L. W. (2011) *J. Mol.*

Biol. **406**, 503-515
26. Karala, A. R., Lappi, A. K., Saaranen, M. J., and Ruddock, L. W. (2009) *Antioxid. Redox Signal.* **11**, 963-970
27. Saaranen, M., Karala, A. R., Lappi, A. K., and Ruddock, L. W. (2010) *Antioxid. Redox Signal.* **12**, 15-25
28. Zito, E., Chin, K.-T., Blais, H., and Ron, D. (2010) *J. Cell Biol.* **188**, 821-832
29. Hatahet, F., Ruddock, L. W., Ahn, K., Benham, A., Craik, D., Ellgaard, L., Ferrari, D., and Ventura, S. (2009) *Antioxid. Redox Signal.* **11**, 2807-2850
30. Ellgaard, L., and Ruddock, L. W. (2005) *EMBO Rep.* **6**, 28-32
31. Marciniak, S. J., Yun, C. Y., Oyadomari, S., Novoa, I., Zhang, Y., Jungreis, R., Nagata, K., Harding, H. P., and Ron, D. (2004) *Genes Dev.* **18**, 3066-3077
32. Harding, H. P., Zhang, Y., Zeng, H., Novoa, I., Lu, P. D., Calfon, M., Sadri, N., Yun, C., Popko, B., Paules, R., Stojdl, D. F., Bell, J. C., Hettmann, T., Leiden, J. M., and Ron, D. (2003) *Mol. Cell* **11**, 619-633
33. Haynes, C. M., Titus, E. A., and Cooper, A. A. (2004) *Mol. Cell* **15**, 767-776
34. Chambers, J. E., Tavender, T. J., Oka, O. B., Warwood, S., Knight, D., and Bulleid, N. J. (2010) *J. Biol. Chem.* **285**, 29200-29207
35. Wang, L., Li, S. J., Sidhu, A., Zhu, L., Liang, Y., Freedman, R. B., and Wang, C. C. (2009) *J. Biol. Chem.* **284**, 199-206
36. Dong, G., Wearsch, P. A., Peaper, D. R., Cresswell, P., and Reinisch, K. M. (2009) *Immunity* **30**, 21-32
37. Mariappan, M., Radhakrishnan, K., Dierks, T., Schmidt, B., and von Figura, K. (2008) *J. Biol. Chem.* **283**, 6375-6383
38. Anelli, T., Alessio, M., Bachi, A., Bergamelli, L., Bertoli, G., Camerini, S., Mezghrani, A., Ruffato, E., Simmen, T., and Sitia, R. (2003) *EMBO J.* **22**, 5015-5022
39. Cortini, M., and Sitia, R. (2010) *Traffic* **11**, 651-659
40. Bertoli, G., Simmen, T., Anelli, T., Molteni, S. N., Fesce, R., and Sitia, R. (2004) *J. Biol. Chem.* **279**, 30047-30052
41. Tsuchiya, Y., Kinoshita, K., and Nakamura, H. (2006) *Protein Eng. Des. Sel.* **19**, 421-429
42. Kanamori, E., Murakami, Y., Tsuchiya, Y., Standley, D. M., Nakamura, H., and Kinoshita, K. (2007) *Proteins* **69**, 832-838
43. Anelli, T., Alessio, M., Mezghrani, A., Simmen, T., Talamo, F., Bachi, A., and Sitia, R. (2002) *EMBO J.* **21**, 835-844
44. Fraldi, A., Zito, E., Annunziata, F., Lombardi, A., Cozzolino, M., Monti, M., Spampanato, C., Ballabio, A., Pucci, P., Sitia, R., and Cosma, M. P. (2008) *Hum. Mol. Genet.* **17**, 2610-2621
45. Wang, L., Vavassori, S., Li, S., Ke, H., Anelli, T., Degano, M., Ronzoni, R., Sitia, R., Sun, F., and Wang, C. C. (2008) *EMBO Rep.* **9**, 642-647

46. Klappa, P., Ruddock, L. W., Darby, N. J., and Freedman, R. B. (1998) *EMBO J.* **17**, 927-935
47. Tsai, B., Rodighiero, C., Lencer, W. I., and Rapoport, T. A. (2001) *Cell* **104**, 937-948
48. Byrne, L. J., Sidhu, A., Wallis, A. K., Ruddock, L. W., Freedman, R. B., Howard, M. J., and Williamson, R. A. (2009) *Biochem. J.* **423**, 209-217
49. Denisov, A. Y., Maattanen, P., Dabrowski, C., Kozlov, G., Thomas, D. Y., and Gehring, K. (2009) *FEBS J.* **276**, 1440-1449
50. Vitu, E., Kim, S., Sevier, C. S., Lutzky, O., Heldman, N., Bentzur, M., Unger, T., Yonda, M., Kaiser, C. A., and Fass, D. (2010) *J. Biol. Chem.* **285**, 18155-18165
51. Serve, O., Kamiya, Y., Maeno, A., Nakano, M., Murakami, C., Sasakawa, H., Yamaguchi, Y., Harada, T., Kurimoto, E., Yagi-Utsumi, M., Iguchi, T., Inaba, K., Kikuchi, J., Asami, O., Kajino, T., Oka, T., Nakasako, M., and Kato, K. (2010) *J. Mol. Biol.* **396**, 361-374
52. Nakasako, M., Maeno, A., Kurimoto, E., Harada, T., Yamaguchi, Y., Oka, T., Takayama, Y., Iwata, A., and Kato, K. (2010) *Biochemistry* **49**, 6953-6962
53. Nguyen, V. D., Wallis, K., Howard, M. J., Haapalainen, A. M., Salo, K. E., Saaranen, M. J., Sidhu, A., Wierenga, R. K., Freedman, R. B., Ruddock, L. W., and Williamson, R. A. (2008) *J. Mol. Biol.* **383**, 1144-1155
54. Wang, C., Chen, S., Wang, X., Wang, L., Wallis, A. K., Freedman, R. B., and Wang, C. C. (2010) *J. Biol. Chem.* **35**, 26788-26797

Figure legends

Fig. 1 Docking simulation for the human Ero1α–PDI binary complex

(A) Predicted model of the Ero1α-PDI complex. Using the website (http://sysimm.ifrec.osaka-u.ac.jp/surFit/index.html), full-length human Ero1α and the b-b' domain fragment of human PDI were docked, and the resultant structure is represented by ribbon diagram. The FAD molecule in Ero1α is shown by small yellow-orange spheres. The square indicates the interface of these two enzymes, which is highlighted in (B). On the basis of the whole structure of yeast Pdi1p and the biochemical results obtained so far, the PDI a- and a'- domains are putatively placed in the complex model, in which the redox-active sites of PDI are shown by larger dark yellow spheres. Note that the redox-active site in the PDI a'-domain is predicted to reside close to the shuttle loop of Ero1α (red dotted line).

(B) Stereo view of the interface of the Ero1α-PDI non-covalent interaction. The side chains of Trp272 from Ero1α and its neighboring Phe240, Phe249 and Phe304 from PDI are shown by sticks.

(C) Superposition of crystal structures of human Ero1α (green, PDB ID: 3AHR) and yeast Ero1p (magenta, PDB ID: 2B5E). These two structures are superposed such that the RMSD of their C_α atoms is minimized. The square indicates the protruding β-hairpin regions of Ero1s. Note that the protruding β-hairpin of yeast Ero1p is much shorter than that of human Ero1α.

Fig. 2 In vitro analysis of Ero1α-PDI interaction

(A) Affinity measurements between human PDI and hyperactive (left) or Δ272-274 (right) Ero1α by SPR. The Ero1α constructs were immobilized on a biosensor chip, and various concentrations of PDI were injected as analyte in the presence of 1 mM GSH and 0.25 mM GSSG.

(B) Oxygen consumption by hyperactive Ero1α during oxidation of human PDI mutants in the presence of 10 mM GSH. A control reaction monitoring oxygen consumption in the absence of PDI (GSH/ Ero1α only) is as indicated (black line).

(C) Oxygen consumption by hyperactive or Δ272-274 Ero1α during oxidation of WT PDI in the presence of 10 mM GSH. A control reaction monitoring oxygen consumption in the absence of Ero1α (GSH/PDI only) is as indicated.

(D) Oxygen consumption by Ero1α W272 mutants during oxidation of WT PDI in the presence of 10 mM GSH.

(E) CD spectra in the far UV region of hyperactive (red), W272G (brown), W272E (blue) and Δ272-274 (purple) Ero1α mutants. Spectra were recorded in 20 mM sodium phosphate (pH8.0), 100 mM NaCl. Sample concentration was 2 μM.

Fig. 3 *In vivo* analysis of the functional Ero1α-PDI interaction

(A) *In vivo* oxidative folding of JcM in the presence of co-expressed WT or Δ272-274 Ero1α.

48 hrs after transfection of JcM and either of the indicated Ero1α constructs, HeLa cells were treated with 5 mM DTT for 5 min, washed, and then cultured at 20 °C for the indicated time points without the reducing agent. Aliquots from cell lysates were resolved by non-reducing SDS-PAGE and immunoblotted using anti-J-chain antibodies. Upon DTT removal, reduced JcM (Red.) and JcM dimer (Dim.) fold in more compact species via formation of intrachain disulfides, or form high molecular weight complexes (HMWC) via interchain disulfides.

(B) The graph (n=3-4, mean ± SEM) reports the disappearance of fully reduced monomeric J-chain (Red. in panel A), quantified by densitometry and plotted as the per cent remaining at each time point relative to 0 min. WT Ero1α (green) is more efficient in accelerating JcM oxidation than Δ272-274 Ero1α (cyan). Similar results were obtained by quantifying the formation of HMWC, as well as oxidised monomers and homodimers (not shown).

(C) Aliquots from cell lysates (corresponding to samples in lanes 1, 5, 9 of panel A) were resolved in reducing conditions and immunodecorated with anti-Myc. Note that WT and Δ272-274 Ero1αs were expressed in similar amount, as were JcM.

(D) Different Ox1/Ox2 ratio and mixed disulfide formation in WT and Δ272-274 Ero1α. HeLa cells co-transfected with PDI and myc-tagged WT or Δ272-274 Ero1α were analyzed by SDS-PAGE under reducing (R) and non-reducing (NR) conditions, and immunoblotted with anti-Myc (top panels) or anti-PDI (bottom panels). The different redox isoforms of Ero1α (Ox1 and Ox2) and Ero1α–PDI covalent complexes are indicated on the right hand margin.

(E) Densitometric quantification of Ox1 and Ox2 forms reveals a higher Ox1/Ox2 ratio in WT Ero1α than in Δ272-274 Ero1α (mean of 3 independent experiments ± SEM).

Fig. 4 Redox-dependent interaction of PDI with Ero1α

(A) Redox states of WT PDI and hyperactive Ero1α in the presence of different redox reagents. Samples were incubated in buffers containing the indicated redox reagents for 30 min at room temperature. After TCA precipitation and subsequent cysteine alkylation with maleimidyl-PEG 2,000 (for PDI) or AMS (for Ero1α), samples were resolved electrophoretically under non-reducing conditions.

(B) SPR affinity measurements between hyperactive Ero1α and WT (top panels) or Cys-less PDI (bottom panels) in the presence of 1mM GSH/0.25 mM GSSG (left panels) or 2mM GSSG (right panels). The lowest panel summarizes the kinetic parameters calculated for binding of the PDI constructs to hyperactive Ero1α under each redox condition.

Fig. 5 Different binding modes of Ero1α toward ERp44 and PDI

(A) SPR affinity measurements between human ERp44 and hyperactive (left) or Δ272-274 (right) Ero1α. The Ero1α constructs were immobilized on a biosensor chip, and various concentrations of ERp44 were injected as an analyte in the presence of 1 mM GSH and 0.25 mM GSSG. Calculated kinetic parameters for binding of human ERp44 to

hyperactive or Δ272-274 Ero1α are compiled in the lower panel.

(B) Co-immunoprecipitation of PDI or ERp44 with co-transfected WT or Δ272-274 Ero1α-Myc. Immunoprecipitates using an anti-Myc antibody were subjected to reducing SDS-PAGE and analyzed by immunoblotting with anti-Myc (upper), anti-PDI (middle) and anti-ERp44 (lower) antibodies.

(C) Oxygen consumption by hyperactive Ero1α during oxidation of PDI in the presence or absence of 50 μM WT ERp44.

Fig. 6 An ERp44 mutant lacking the C-terminal tail-deleted (ΔTail ERp44) inhibits JcM oxidation in cells.

(A) Oxygen consumption by hyperactive Ero1α during oxidation of PDI in the presence or absence of 10 μM ΔTail ERp44. Note that addition of the ERp44 mutant substantially inhibited Ero1α activity.

(B) *In vivo* oxidative folding of JcM in the presence of co-expressed WT or ΔTail ERp44. Experimental procedures are essentially the same as in Fig. 3A. The part of the gel corresponding to reduced JcM is shown for clarity.

(C) SPR affinity measurements between ΔTail ERp44 and hyperactive (left) or Δ272-274 (right) Ero1α. Calculated kinetic parameters for binding of ΔTail ERp44 to hyperactive or Δ272-274 Ero1α are compiled in the lower panel.

Fig. 7 Model of the Ero1α-PDI pathway sustaining oxidative protein folding

The Ero1α-PDI catalytic cycle proceeds in the following order of events. (i) Reduced PDI binds Ero1α through the specific interaction between the hydrophobic pocket in the PDI b'-domain and the protruding β-hairpin of Ero1α such that the redox active site of the PDI a'-domain is preferentially oxidized by Ero1α. (ii) Once oxidized, PDI converts to the conformation with a more exposed hydrophobic pocket through the conformational change of the x-linker region and the subsequent relocation of the a'-domain relative to the b'-domain. Oxidized PDI has lower affinity for Ero1α than for unfolded substrate proteins. (iii) Consequently, an unfolded protein displaces Ero1α, and undergoes PDI-catalyzed oxidation. (iv) If correctly folded, the protein dissociates from reduced PDI, which can reenter into step (i) for oxidation by Ero1α. Should a non-native disulfide be inserted into the substrate, reduced PDI or other PDI-family member proteins could act as an isomerase.

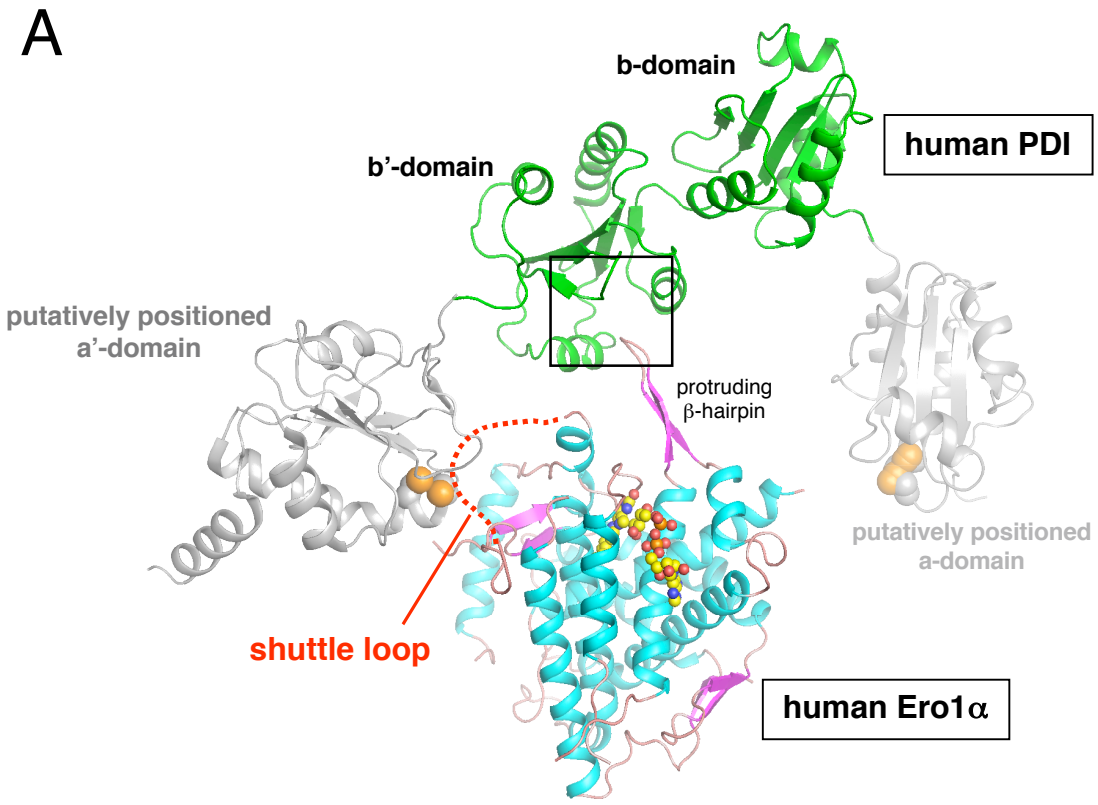

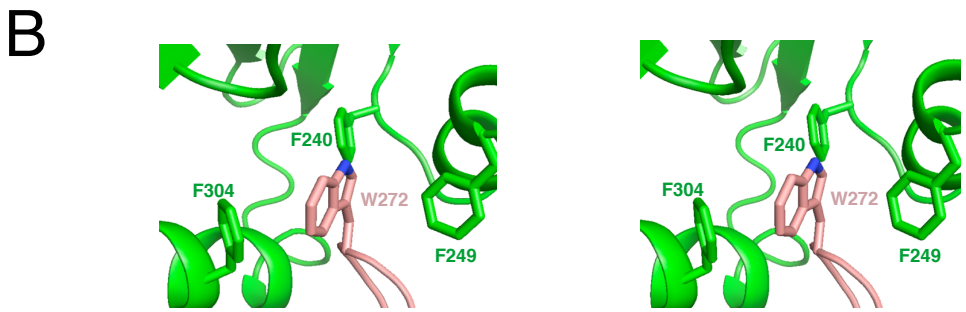

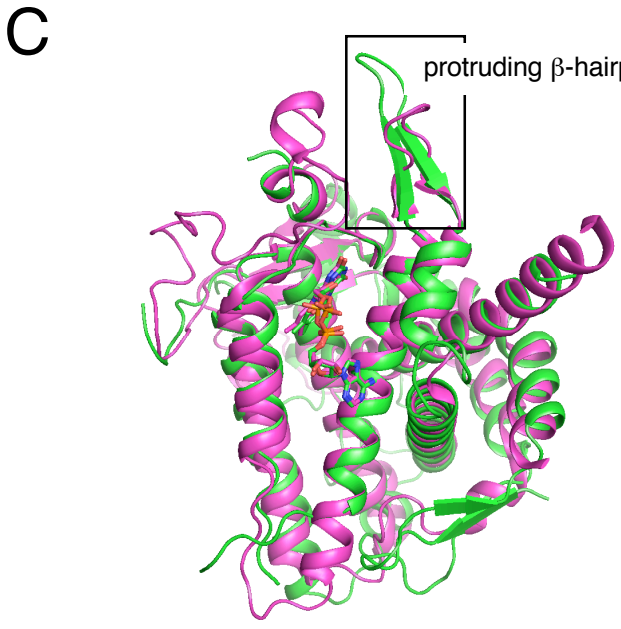

Fig.1 Masui et al.

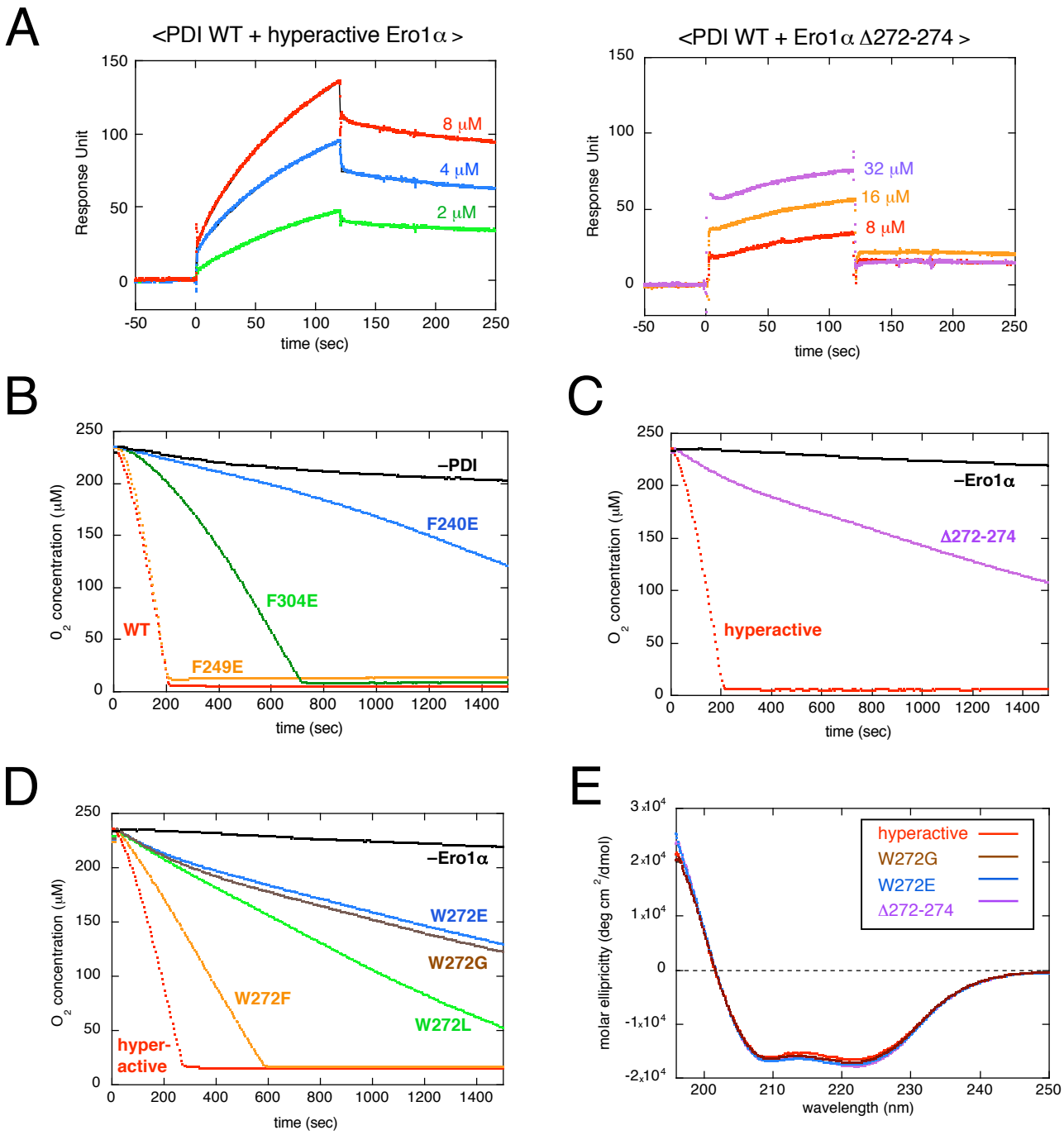

Fig.2 Masui et al.

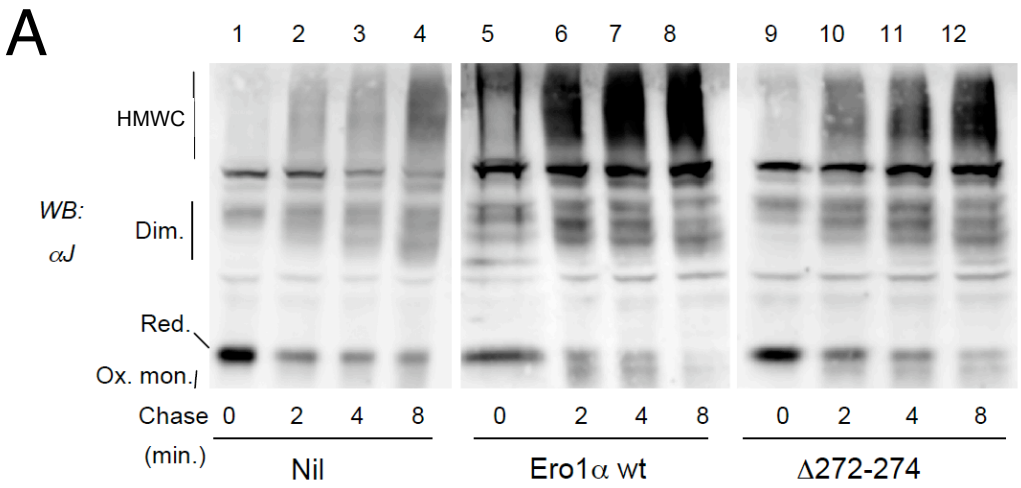

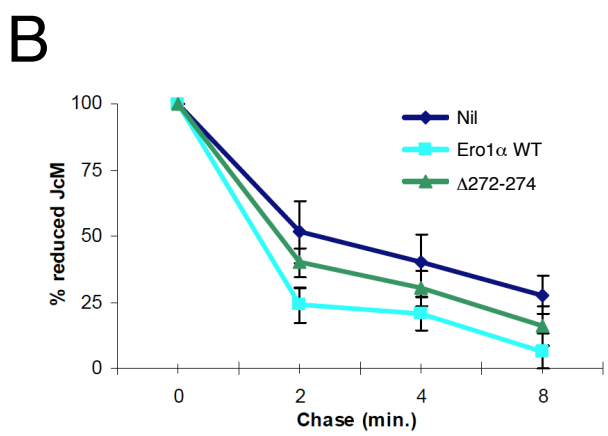

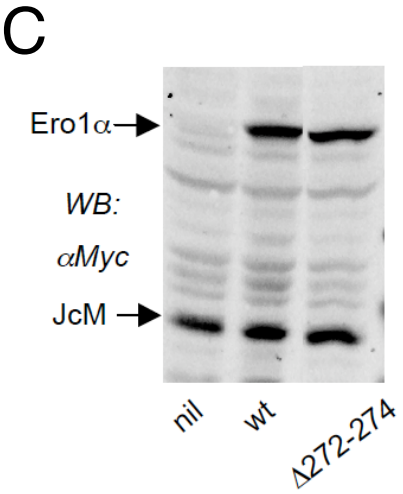

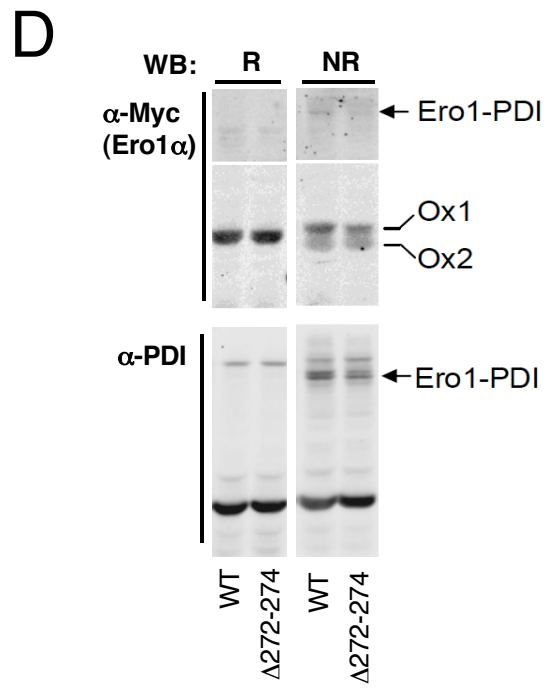

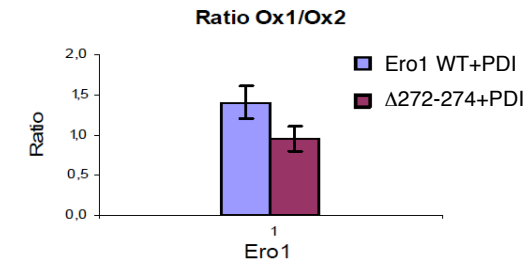

Fig. 3 Masui et al.

A

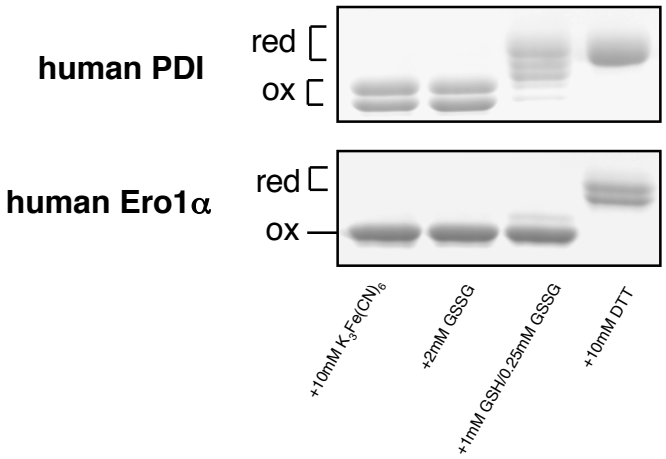

B

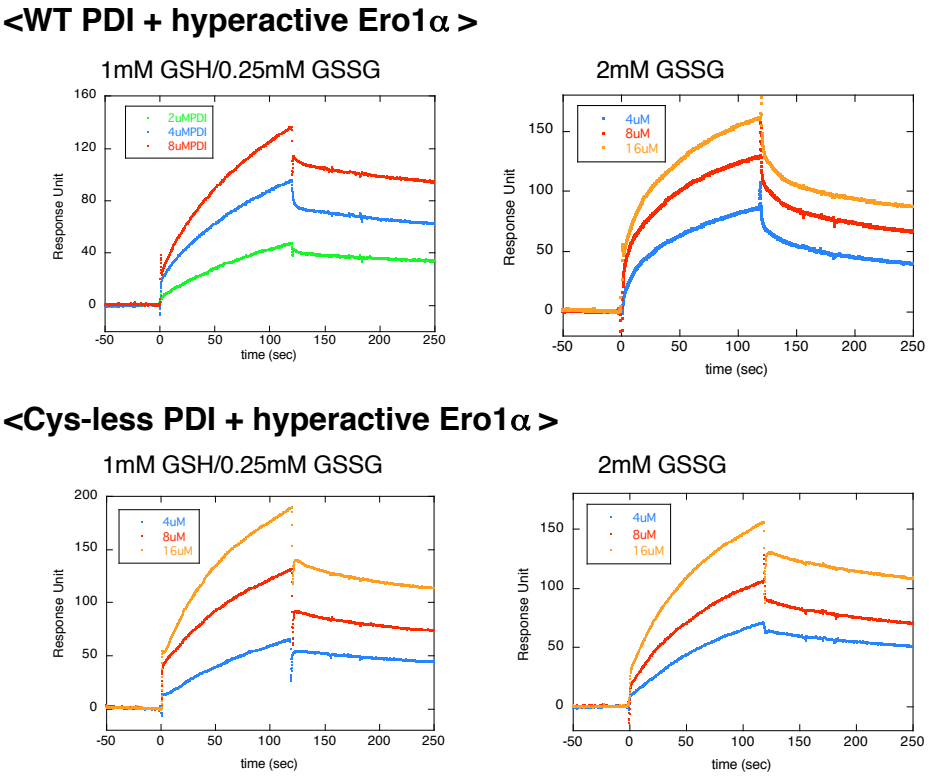

	k_{on} ($M^{-1}s^{-1}$)	k_{off} (s^{-1})	K_D (M)
WT PDI + hyperactive Ero1α			
1mM GSH/0.25mM GSSG	2.0 ± 0.0 x10^3	4.1 ± 0.2 x10^{-3}	2.1 ± 0.1 x10^{-6}
2mM GSSG	2.1 ± 0.0 x10^3	5.6 ± 0.1 x10^{-2}	2.7 ±0.1 x10^{-5}
Cys-less PDI + hyperactive Ero1α			
1mM GSH/0.25mM GSSG	0.8 ± 0.0 x10^3	4.4 ± 0.1 x10^{-3}	5.5 ± 0.2 x10^{-6}
2mM GSSG	1.2 ± 0.0 x10^3	4.9 ± 0.4 x10^{-3}	4.1 ± 0.4 x10^{-6}

Fig. 4 Masui et al.

A

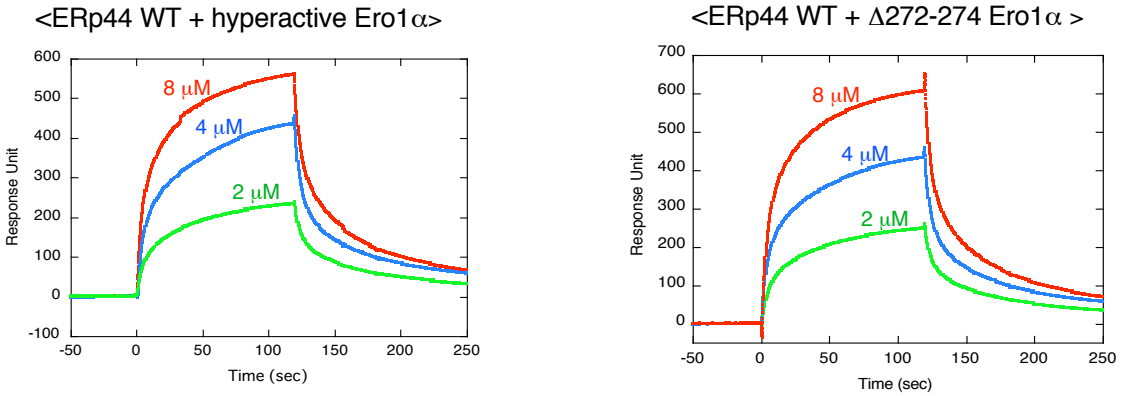

	k_{on} ($M^{-1}s^{-1}$)	k_{off} (s^{-1})	K_D (M)
ERp44 WT + hyperactive Ero1α	2.2 ± 0.0 x10^{3}	8.9 ± 0.1 x10^{-2}	4.0 ± 0.1 x10^{-5}
ERp44 WT + Δ272-274 Ero1α	2.1 ± 0.0 x10^{3}	9.5 ± 0.1 x10-^{2}	4.5 ± 0.1 x10^{-5}

B

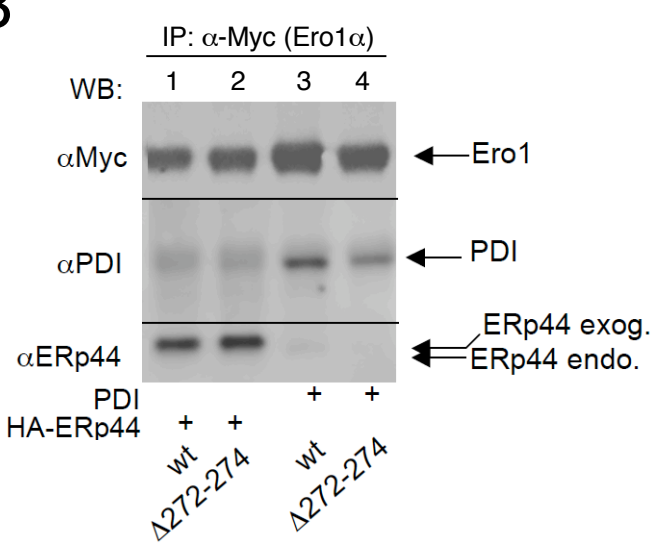

C

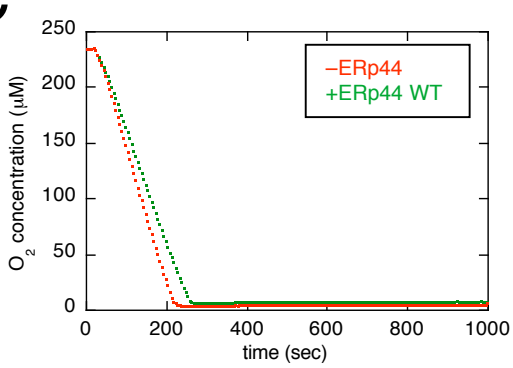

Fig. 5 Masui et al.

A

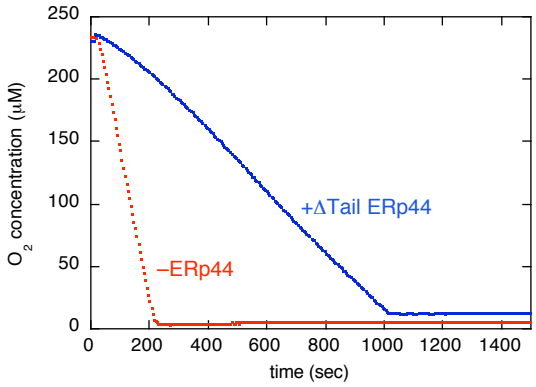

B

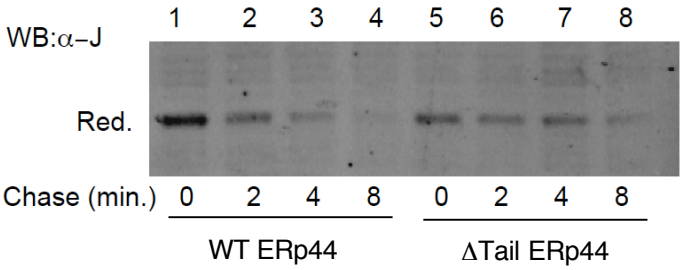

C

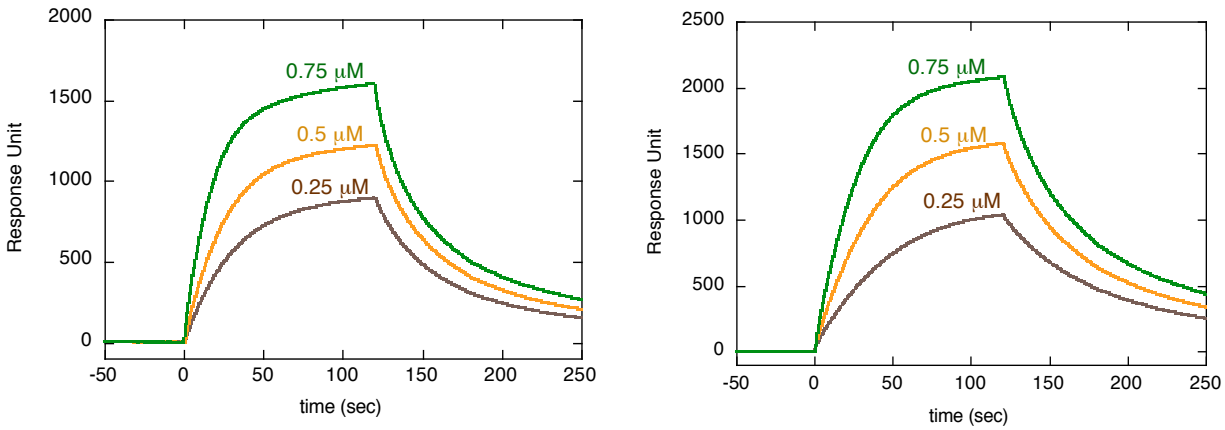

	k_{on} ($M^{-1}s^{-1}$)	k_{off} (s^{-1})	K_D (M)
ΔTail ERp44 + hyperactive Ero1α	4.7 ± 0.0 x10^{4}	2.2 ± 0.1 x10^{-2}	4.7 ± 0.1 x10^{-7}
ΔTail ERp44 + Δ272-274 Ero1α	2.9 ± 0.1 x10^{4}	1.8 ± 0.0 x10^{-2}	6.2 ± 0.1 x10^{-7}

Fig. 6 Masui et al.

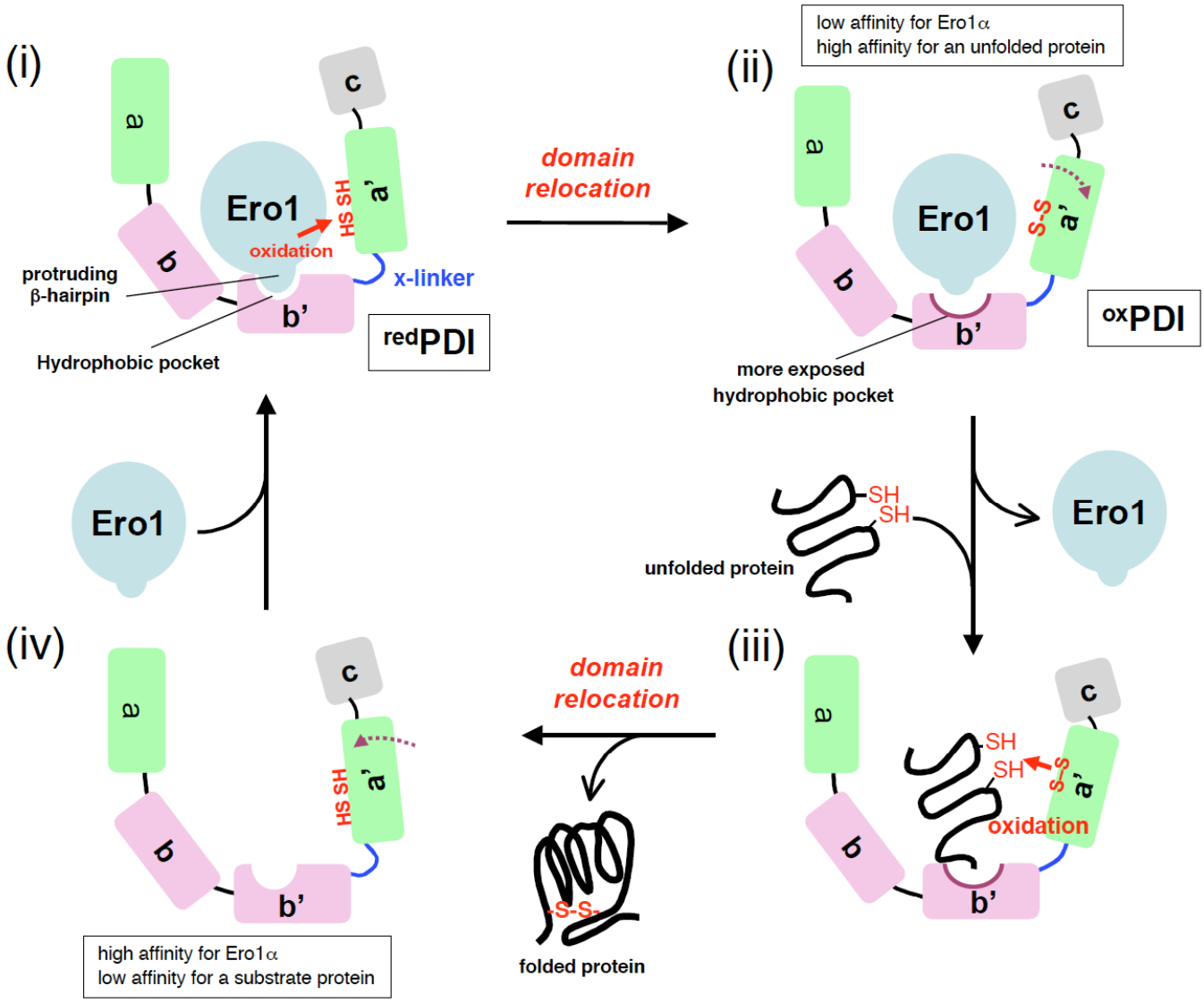

Fig. 7 Masui et al.